JOURNAL OF APPLIED ELECTROCHEMISTRY 17 (1987) 113–122

Simulation and optimization of a packed bipolar cell by means of a combination of conducting paper and an electric model circuit

YOSHINORI MIYAZAKI[1], AKIRA KATAGIRI[2], SHIRO YOSHIZAWA[1]

[1]*Department of Industrial Chemistry, Faculty of Engineering, and* [2]*Department of Chemistry, College of Liberal Arts and Sciences, Kyoto University, Sakyo-ku, Kyoto 606, Japan*

Received 2 September 1985; revised 21 March 1986

The potential distribution and current distribution in a packed bipolar cell were simulated using conducting paper and an electric model circuit. Conducting paper was cut to a pattern which represented an electrolyte solution, while an electric circuit was used which simulated the current–potential relationship at the electrode–electrolyte interface. The potential distribution measured on the paper pattern was not as uniform as expected from the linear field model, particularly when the faradaic current was small. The effective electrode area and the power efficiency were measured under different conditions. The similarity law was confirmed to hold when parameters characterizing the cell were kept constant. Procedures for optimization of the cell design and operating conditions are discussed.

Nomenclature

A	effective electrode area (cm)*
A_T	half the total surface area of cylindrical electrode (cm)*
a	length of unit cell (cm)
E	average electric field in solution ($V\,cm^{-1}$)
I_F	faradaic current in unit cell (A)
I_S	by-pass current through solution in unit cell (A)
I_T	total current in unit cell (A)
i_a	anodic limiting current density ($A\,cm^{-1}$)*
i_c	cathodic limiting current density ($A\,cm^{-1}$)*
i_d	limiting current density ($A\,cm^{-1}$)*
K_a	dimensionless parameter, $i_a a/V_0\kappa$
K_c	dimensionless parameter, $i_c a/V_0\kappa$
K	dimensionless parameter, $i_d a/V_0\kappa$
r	radius of cylindrical electrode (cm)
V_0	threshold voltage (V)
V_{cell}	voltage applied to unit cell (V)
x, y	Cartesian coordinates defined in Fig. 1 (cm)
X, Y	Dimensionless variables corresponding to x and y
α	dimensionless parameter, r/a
ε	dimensionless parameter, Ea/V_0
η_P	power efficiency (dimensionless)
θ	angle defined in Fig. 1 (radian)
κ	specific conductivity of solution or conducting paper (Ω^{-1})*
ϕ_m	inner potential of metal (V)
$\phi_s(x, y)$	inner potential of solution (V)
$\Delta\phi_a$	inner potential difference defined in Fig. 2 (V)
$\Delta\phi_c$	inner potential difference defined in Fig. 2 (V)
$\Phi(X, Y)$	dimensionless function defined by Equation 12

* These units correspond to the two-dimensional model.

0021–891X/87 $03.00 + .12

1. Introduction

The packed bipolar cell is a type of electrolytic cell in which a large number of conducting particles are placed between the main electrodes, and a sufficiently high field is applied so that each particle behaves as a bipolar electrode [1]. Since numerous unit cells are formed in the space between the main electrodes, reactants can easily reach the reaction areas. Therefore, this type of cell is suitable for the electrolysis of solutions of low reactant concentration, for which the mass transport problem is serious in conventional cells. The packed bipolar cell is also advantageous in the electrolysis of solutions of low electric conductivity since the ohmic loss is small due to the small gaps between the packing particles. This type of cell has been tested in the electrolytic treatment of waste waters [2–6] and in the electrosynthesis of organic chemicals such as propylene oxide and styrene oxide [1, 7].

We have studied the behaviour of a model bipolar cell which consisted of graphite rods as bipolar electrodes [8]. In the analysis of the cell performance we have applied a simplified model which is based on the concept of threshold voltage and on the assumption of a linear potential gradient in the solution [1, 7]. However, the analysis was not very satisfactory; the predicted values of the power efficiency did not agree well with the observed values. It seemed necessary to investigate the potential distribution and the current distribution in solution instead of assuming a linear potential gradient in the solution.

The current distribution in electrolytic cells has been one of the major concerns in electrochemical engineering [9–12]. Thus, primary and secondary current distributions have been calculated in cells of simple geometry. The use of conducting paper with uniform conductivity has been proposed for simulating the primary current distribution in cells of complex geometry. In the present work we propose a new method of simulating the current distribution in a packed bipolar cell by using a combination of conducting paper and an electric model circuit, and also describe procedures for the optimization of the cell design and operating conditions.

2. Theory

2.1. *Principle of similarity of the potential distribution*

In order to simulate the potential distribution in a packed bipolar cell and to analyse cell characteristics such as effective electrode area and power efficiency, a simplified two-dimensional model is used. Thus, a three-dimensional bed of conducting particles is represented by an array of conducting cylinders which are arranged parallel to each other with a square lattice configuration in an electrolytic solution, as shown in Fig. 1. When a sufficiently large electric field is applied in the solution each cylinder becomes a bipolar electrode; anodic and cathodic reactions take place on the opposite sides of each cylinder. We assume a simplified current–potential relationship as shown in Fig. 2. Thus, an anodic reaction occurs at a limiting current density of i_a when $\phi_m - \phi_s$ is larger than $\Delta\phi_a$, and a cathodic reaction occurs at a limiting current density of i_c when $\phi_m - \phi_s$ is smaller than $\Delta\phi_c$, where ϕ_m and ϕ_s are the inner potentials of the cylinder (electronic conductor) and the

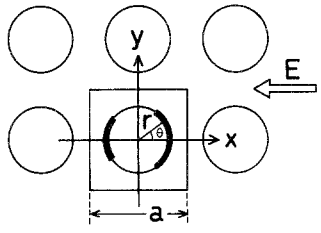

Fig. 1. Two-dimensional model of the packed bipolar cell.

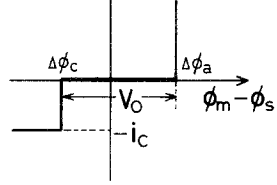

Fig. 2. Model of the current–potential relationship.

solution (ionic conductor), respectively. The difference between $\Delta\phi_a$ and $\Delta\phi_c$ is the so-called 'threshold voltage' (V_0) which has been defined by Fleischmann *et al.* [1]. The anodic and cathodic limiting currents may be caused either by diffusion of some reacting species or by kinetics of some chemical reaction. Although it is not realistic to assume such a current–potential relationship, particularly the case where $i_a = i_c$ as described later, the following idea and technique may be helpful to understand typical characteristics of a packed bipolar cell. The technique can be modified to other types of current–potential relationships, e.g. a Tafel-type relationship.

We now consider the potential distribution in the solution in a unit cell shown in Fig. 1, using the two-dimensional Cartesian coordinates. The potential of solution $\phi_s(x, y)$ is expressed by the Laplace equation

$$\frac{\partial^2\phi_s(x, y)}{\partial x^2} + \frac{\partial^2\phi_s(x, y)}{\partial y^2} = 0 \tag{1}$$

which must satisfy the following boundary condition

$$\left[\frac{\partial\phi_s(x, y)}{\partial y}\right]_{y=\pm a/2} = 0 \tag{2}$$

Since $\phi_s(x, y)$ is a cyclically changing function with respect to x, it is expressed as

$$\phi_s(x, y) = \phi_s(x - a, y) + Ea \tag{3}$$

Since the cylinders have high electronic conductivity, ϕ_m is assumed to be constant throughout each cylinder. A boundary condition at the surface of the cylinder is given by the following equation:

$$\kappa\left[\frac{\partial\phi_s(x, y)}{\partial x}\cos\theta + \frac{\partial\phi_s(x, y)}{\partial y}\sin\theta\right]_{CS} = \left\{\begin{array}{ll} i_c & \text{when } \phi_m - \phi_s(x, y) < \Delta\phi_c \\ 0 & \text{when } \Delta\phi_c < \phi_m - \phi_s(x, y) < \Delta\phi_a \\ -i_a & \text{when } \Delta\phi_a < \phi_m - \phi_s(x, y) \end{array}\right\} \tag{4}$$

where the subscript CS denotes the surface of the cylinder, that is, $x^2 + y^2 = r^2$. The variable, θ, may be regarded as a function of x and y, that is, $\theta = \tan^{-1}(y/x)$. As the anodic and cathodic currents must cancel each other, the following equation should hold:

$$\int_0^{2\pi}\kappa\left[\frac{\partial\phi_s(x, y)}{\partial x}\cos\theta + \frac{\partial\phi_s(x, y)}{\partial y}\sin\theta\right]_{CS} r\,d\theta = 0 \tag{5}$$

In principle, the potential distribution is obtained by solving the differential equation (Equation 1) under the limiting conditions of Equations 2–5. However, analytical solution is difficult as is numerical solution.

Now we consider the necessary conditions for the existence of the similarity law with respect to the potential distribution. We define dimensionless parameters as follows:

$$\alpha = r/a \tag{6}$$

$$K_a = i_a a/V_0\kappa \tag{7}$$

$$K_c = i_c a/V_0\kappa \tag{8}$$

$$\varepsilon = Ea/V_0 \tag{9}$$

If x, y and $\phi_s(x, y)$ are replaced by the dimensionless variables X, Y and $\Phi(X, Y)$, which are defined by

$$X = x/a \tag{10}$$

$$Y = y/a \tag{11}$$

$$\Phi(X, Y) = [\phi_s(x, y) - \phi_m + (\Delta\phi_a + \Delta\phi_c)/2]/V_0 \tag{12}$$

then, the following equations are derived from Equations 1–5:

$$\frac{\partial^2\Phi(X, Y)}{\partial X^2} + \frac{\partial^2\Phi(X, Y)}{\partial Y^2} = 0 \tag{13}$$

$$\left[\frac{\partial\Phi(X, Y)}{\partial Y}\right]_{Y=\pm 1/2} = 0 \tag{14}$$

$$\Phi(X, Y) = \Phi(X - 1, Y) + \varepsilon \tag{15}$$

$$\left[\frac{\partial\Phi(X, Y)}{\partial X}\cos\theta + \frac{\partial\Phi(X, Y)}{\partial Y}\sin\theta\right]_{CS} = \left\{\begin{array}{ll} K_c & \text{when } \frac{1}{2} < \Phi \\ 0 & \text{when } -\frac{1}{2} < \Phi < \frac{1}{2} \\ -K_a & \text{when } \Phi < -\frac{1}{2} \end{array}\right\} \tag{16}$$

$$\int_0^{2\pi}\left[\frac{\partial\Phi(X, Y)}{\partial X}\cos\theta + \frac{\partial\Phi(X, Y)}{\partial Y}\sin\theta\right]_{CS} d\theta = 0 \tag{17}$$

In this case the subscript CS represents the condition $X^2 + Y^2 = \alpha^2$. In principle, the function $\Phi(X, Y)$ is determined by Equations 13–17 which contain the dimensionless parameters α, K_a, K_c and ε. Therefore, it is concluded that the similarity law holds with respect to the potential distribution when these parameters are kept constant.

If we consider kinetically controlled current–potential relationships for the anodic and/or cathodic reactions, we must define other types of dimensionless parameters, e.g. the parameter which contains the Tafel b-factor for a Tafel-type relationship.

2.2. *Characteristics describing the performance of packed bipolar cell*

An important quantity which characterizes a packed bipolar cell is the effective electrode (cathode or anode) area on each packing particle. This quantity determines the production capacity of the cell. If the above two-dimensional model is employed and if a symmetric current–potential relationship is assumed, i.e. $i_a = i_c$, then the effective electrode area, A, increases with increasing field, approaching half the surface area of the cylinder, A_T. The fraction A/A_T is therefore a convenient quantity describing the cell performance, although it can approach a value different from one when $i_a \neq i_c$. Since the potential distribution, and therefore the current distribution, are determined by the parameters α, K_a, K_c and ε, the fraction A/A_T is also determined by these four parameters.

In view of the energy requirement in a packed bipolar cell, the power efficiency is another important quantity. If the simplified current–potential relationship shown in Fig. 2 is assumed, the threshold voltage, V_0, is regarded as the minimum voltage for the electrolysis. When no side reaction occurs the power efficiency, η_P, can be defined by

$$\eta_P = \frac{V_0 I_F}{V_{cell} I_T} \tag{18}$$

where V_{cell} is the voltage applied to the unit cell, i.e. $V_{cell} = Ea$. The power efficiency, η_P, is also determined by the parameters α, K_a, K_c and ε.

3. Technique

Simulation was carried out using a combination of conducting paper and an electric model circuit. (The conducting paper used in this work was 'Anacon Paper' provided by Tomoegawa Seishi, Ltd, which was a sheet of uniformly pressed carbon powder on a paper substrate. The two-dimensional

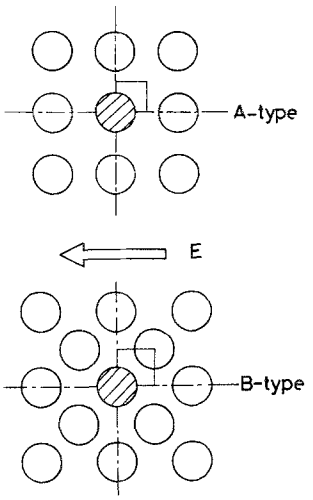

Fig. 3. Two types of arrangements of the cylindrical electrodes.

'specific conductivity' was $2.2 \times 10^{-3}\,\Omega^{-1}$.) The conducting paper represents an electrolytic solution of constant ionic conductivity and the electric model circuit simulates a current–potential relationship at the electrode–electrolyte interface. Two types of arrangements of cylinders were considered, as shown in Fig. 3. A symmetric current–potential relationship was assumed for the anodic and cathodic reactions, i.e. $i_a = i_c\ (= i_d)$ for simplicity. From the consideration of symmetry of the A-type arrangement, it is apparent that the planes perpendicular to the x-axis at $x = 0$ and $x = \pm a/2$ are equipotential surfaces, and the planes perpendicular to the y-axis at $y = 0$ and $y = \pm a/2$ are surfaces in which current lines lie. Similar arguments can be made about the B-type arrangement. Therefore, only the potential distribution in the squares shown in Fig. 3 must be considered. Fig. 4a and b shows the patterns used for the A- and B-type arrangements, respectively.

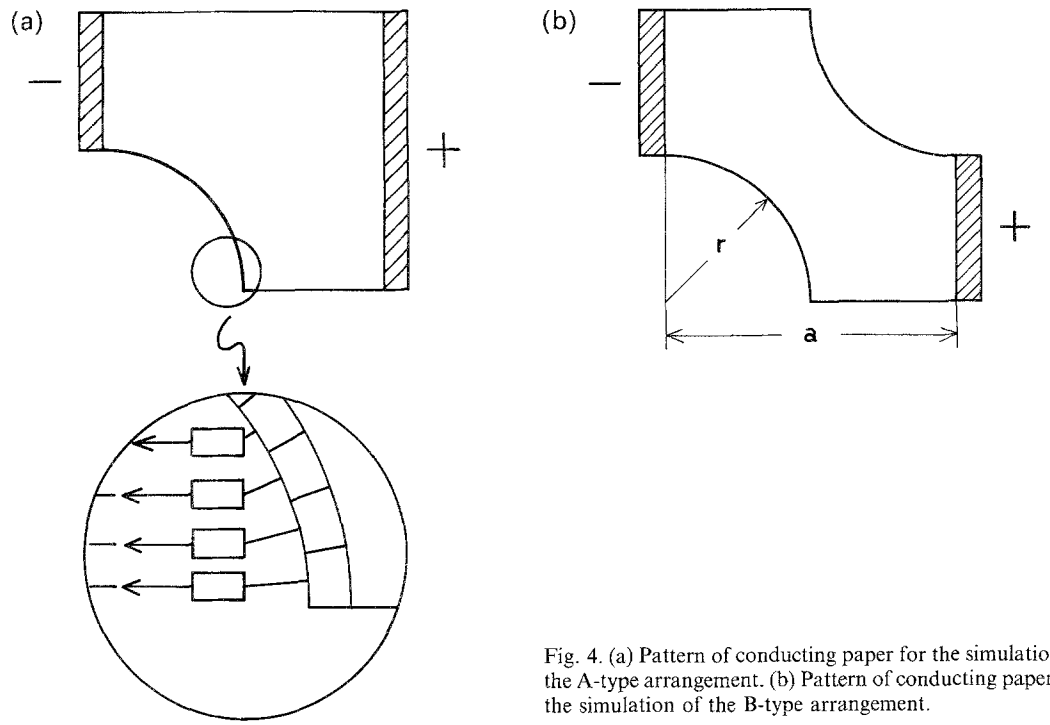

Fig. 4. (a) Pattern of conducting paper for the simulation of the A-type arrangement. (b) Pattern of conducting paper for the simulation of the B-type arrangement.

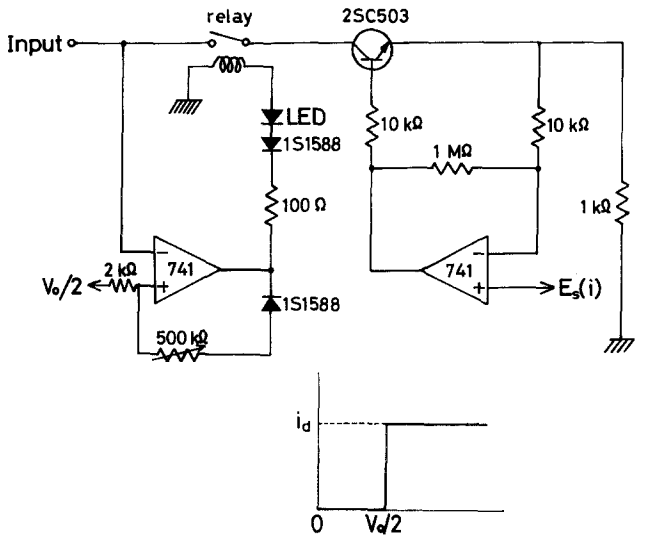

Fig. 5. Electric circuit simulating the current–potential relationship shown in Fig. 2.

In the case of A-type arrangement, a piece of conducting paper was cut to the pattern (Fig. 4a) and conducting paste was put on the side ends (hatched areas) of the paper as electric terminals. The circular end of the paper was divided into nine sections, each of which was connected to a current-controlling unit. Fig. 5 shows the electric circuit of the unit, in which the 'input' terminal was connected to a divided section on the paper and the ground terminal was connected to the negative terminal of the paper (see Fig. 4a). The electric unit allows a constant current to flow if the input voltage is larger than a preset voltage ($V_0/2$), as shown by the current–potential relationship at the bottom of the figure.

In the case of B-type arrangement, a piece of conducting paper was cut to the pattern of Fig. 4b, and two sets of current-controlling units were attached to the divided sections of the circular ends. One set of units which were used on the negative side (cathode) were identical to the one shown in Fig. 5, while the other set used on the positive side (anode) had the same characteristics except that the direction of the current flow and the polarity of the input voltage were inverted.

A constant voltage ($V_{cell}/2$) was applied between the positive and negative terminals of a conducting paper (see Fig. 4a, b). The total current passing through the entire system, which corresponds to half the total current in the unit cell ($I_T/2$), and the current passing through the divided sections of a circular end, which corresponds to half the faradaic current in the unit cell ($I_F/2$), were recorded. The fraction A/A_T was obtained simply by dividing the number of current-flowing sections by the total number of sections (nine). The power efficiency, η_P, was calculated by Equation 18.

Although asymmetric cases ($i_a \neq i_c$) are not treated in this paper, the technique needed is substantially the same as described above. One important difference is that the anodic and cathodic currents must be balanced in the unit cell; this condition is automatically satisfied in the symmetric case ($i_a = i_c$). Furthermore, it is possible to achieve a Tafel-type current–potential relationship by means of an electric circuit which represents the relevant exponential function.

4. Results and discussion

4.1. *Potential distribution*

The potential distribution on the conducting paper was measured by using an electrometer and a probe. Fig. 6 shows equipotential lines obtained for two different values of applied field. It is seen that the pattern of the potential distribution varies with applied field. In the case of low field (left),

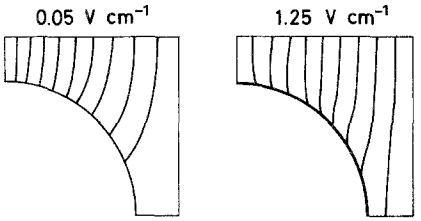

Fig. 6. Potential distribution on the conducting paper for the A-type arrangement. a, 40 cm; r, 15 cm; V_0, 2 V; i_d, 1.1 mA cm^{-1}; κ: 2.2 × 10$^{-3}\Omega^{-1}$. Equipotential lines are drawn at intervals of a tenth of the applied voltage.

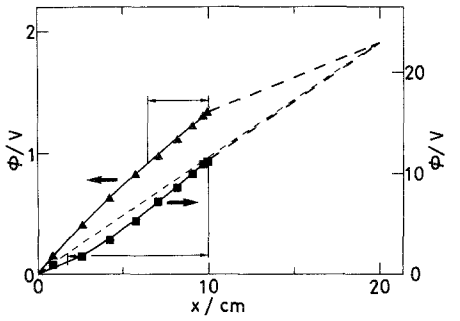

Fig. 7. Potential at the circular end of the conducting paper plotted against x for the A-type arrangement. a, 40 cm; r, 10 cm; V_0, 2 V; κ, 2.2 × 10$^{-3}\Omega^{-1}$; i_d, 0.057 mA cm^{-1} (▲), 2.3 mA cm^{-1} (■); E, 0.095 V cm^{-1} (▲), 1.15 V cm^{-1} (■).

the fraction of the effective electrode area, A/A_T, is so small that the electrode surface (circular end) behaves like an insulator. In the case of high field (right), the equipotential lines lie approximately parallel to the y-axis and at equal separations, as is expected from the linear field model.

Fig. 7 shows the potential of the solution at the electrode surface as a function of x. The thin broken line indicates the potential distribution which is expected from the linear field model. The double-headed arrows indicate the regions corresponding to the effective electrode area. It is noted that a considerable deviation from the linear field model occurs particularly when the faradaic current is small. Generally, potential–distance curves in Fig. 7 lie above the broken line of the linear field model when the by-pass current is predominant over the faradaic current; that is, the current lines concentrate in the by-pass solution. This condition is typically shown in the left hand side of Fig. 6. The reverse situation arises when the current lines concentrate on the electrode surface.

4.2. *Effective electrode area*

Fig. 8 shows the fraction of the effective electrode area A/A_T plotted against the average field, E, for three different values of i_d. As expected, the effective electrode area increases with increasing field but the curves obtained are dependent on i_d. If we assume a linear field in the solution, the effective

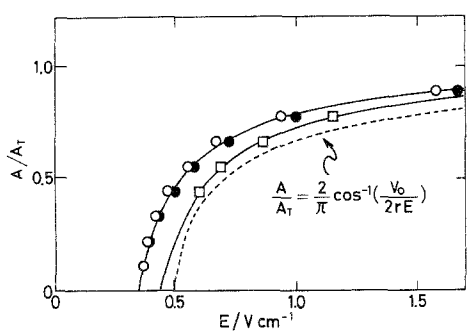

Fig. 8. Fraction of the effective electrode area, A/A_T, against applied field, E for the A-type arrangement. a, 20 cm; r, 10 cm; V_0, 10 V; κ, 2.2 × 10$^{-3}\Omega^{-1}$; i_d, 0.0573 mA cm^{-1} (○), 0.286 mA cm^{-1} (●), 1.15 mA cm^{-1} (□). The broken line represents the relationship of Equation 20.

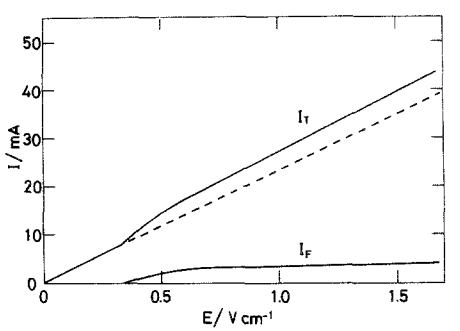

Fig. 9. Faradaic current, I_F, and total current, I_T, in unit cell for the A-type arrangement. a, 20 cm; r, 10 cm; V_0, 10 V; i_d, 0.286 mA cm^{-1}; κ, 2.2 × 10$^{-3}\Omega^{-1}$.

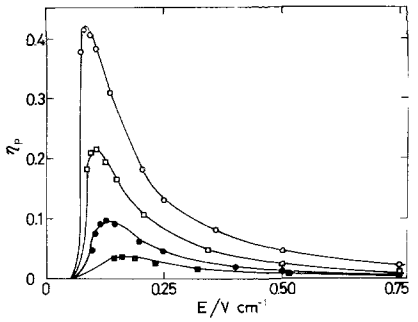

Fig. 10. Power efficiency, η_P, as a function of applied field, E, at different radii, r, of electrode for the B-type arrangement. a, 20 cm; V_0, 2 V; i_d, 0.115 mA cm^{-1}; κ: 2.2 × $10^{-3}\Omega^{-1}$; r, 5 cm (■), 7 cm (●), 10 cm (□), 13 cm (○).

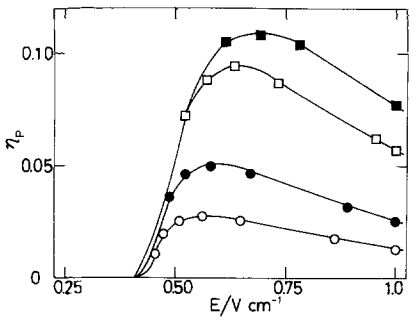

Fig. 11. Power efficiency, η_P, as a function of applied field, E, at different values of i_d for the B-type arrangement. a, 20 cm; r, 7 cm; V_0, 10 V; κ, 2.2 × $10^{-3}\Omega^{-1}$; i_d, 0.115 mA cm^{-1} (○), 0.229 mA cm^{-1} (●), 0.573 mA cm^{-1} (□), 0.819 mA cm^{-1} (■).

electrode area* on a cylinder in the two-dimensional model is given by [7]:

$$A = 2r \cos^{-1}(V_0/2rE) \tag{19}$$

Since A_T is equal to πr, the fraction of the effective electrode area is expressed as:

$$A/A_T = (2/\pi) \cos^{-1}(V_0/2rE) \tag{20}$$

The relationship of Equation 20 is depicted by the broken line in Fig. 8. Although the observed curves are approximately represented by Equation 20, a significant deviation is seen when i_d is small. It is noted that the A/A_T curve shifts to the left in Fig. 8 when the by-pass current is predominant over the faradaic current (see Fig. 6, left).

4.3. *Power efficiency*

Fig. 9 shows an example of the total current, I_T, and the faradiac current, I_F, in the unit cell as functions of applied field. The faradaic current begins to flow at $\sim 0.4\,\mathrm{V\,cm^{-1}}$ and increases with increasing field, approaching a limit. The total current, I_T, is the sum of I_F and I_S, the latter being approximately proportional to the applied field. From data such as that of Fig. 9, the power efficiency, η_P, can be calculated according to Equation 18. Fig. 10 shows η_P against E for different radii of the cylindrical electrode, otherwise under the same conditions. A maximum power efficiency is obtained at a certain field. It is noted that the highest value of η_P is attained at the largest possible value of r for a given value of a. The largest value of the ratio r/a is $1/(2)^{1/2}$ for the B-type arrangement.

Figs 11 and 12 show the η_P–E relationship for different values of i_d and V_0, respectively. The maximum value of η_P and the position of the maximum are dependent on i_d and V_0. As described in Section 2.2, η_P should be determined by the dimensionless parameters $\alpha = r/a$, $K = i_d a/V_0\kappa$ and $\varepsilon = Ea/V_0$. Fig. 13 is a plot of η_P against Ea/V_0 for different values of a when r/a and $i_d a/V_0\kappa$ are kept constant. Fig. 14 shows η_P plotted against Ea/V_0 for different values of V_0 and i_d when r/a and $i_d a/V_0\kappa$ are kept constant. Figs 13 and 14 indicate that the similarity law holds as long as the parameters r/a, $i_d a/V_0\kappa$ and Ea/V_0 are constant. Fig. 15 shows η_P as a function of Ea/V_0 for different values of $i_d a/V_0\kappa$. It is apparent that the highest obtainable value of η_P increases with increasing $i_d a/V_0\kappa$.

Fig. 16 is a comparison of the two different arrangements of cylindrical electrodes of the same size and at the same separations. Although the potential distribution and the current distribution are

* The dimension of 'electrode area' in this two-dimensional model is length.

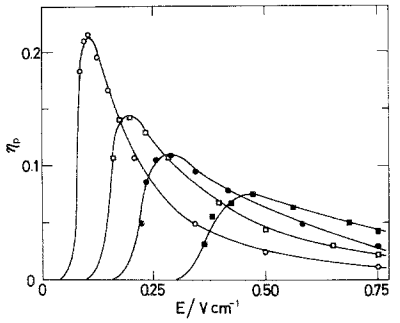

Fig. 12. Power efficiency, η_P, as a function of applied field, E, at different values of V_0, for the B-type arrangement. a, 20 cm; r, 10 cm; i_d, 0.115 mA cm^{-1}; κ, 2.2 × $10^{-3}\Omega^{-1}$; V_0, 2 V; (○), 4 V (□), 6 V (●), 10 V (■).

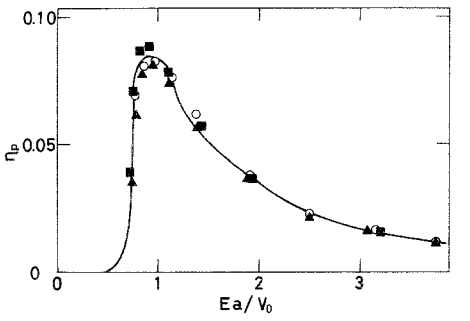

Fig. 13. Power efficiency, η_P, plotted against Ea/V_0 at different values of a for the B-type arrangement. r/a, 0.5; $i_d a/V_0\kappa$, 0.129; a, 10 cm (■), 20 cm (○), 30 cm (▲).

completely different in these two arrangements, the η_P values lie on single curves when the other conditions are the same.

4.4. *Optimization*

In order to design a packed bipolar cell for a certain purpose, we have to determine the optimum conditions of operation. As apparent from Fig. 10, the ratio r/a must be as large as possible to obtain the maximum power efficiency. Thus, the closest packing of particles is desirable. When the properties of the solution and the size of the packing particles are given, the parameter $i_d a/V_0\kappa$ can be calculated and then the optimum field can be determined from the maximum on the relevant $\eta_P - Ea/V_0$ curve such as those in Fig. 15. Fig. 17 shows the relationship between η_P and A/A_T, both of which are regarded as functions of applied field. It is noted that maxima in η_P occur at almost the same value of A/A_T for different values of $i_d a/V_0\kappa$. The fraction A/A_T needs to be about 0.35, irrespective of $i_d a/V_0\kappa$, in order to obtain the maximum power efficiency.

On the other hand, if the space–time-yield (or the amount of material to be removed in unit time and in unit volume of cell) is prescribed instead of a given size of packing particles, then both particle size and applied voltage must be optimized. Thus, the maximum power efficiency should be obtained for a set of r and E values under the condition of the constant space–time yield which is also a function of r and E.

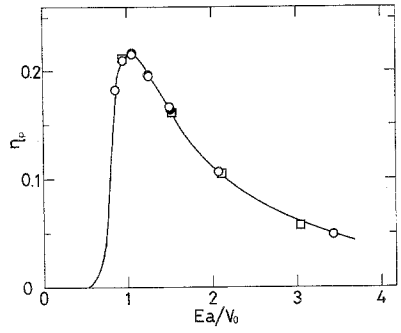

Fig. 14. Power efficiency, η_P, plotted against Ea/V_0 at different values of V_0 and i_d for the B-type arrangement. r/a, 0.5; $i_d a/V_0\kappa$, 0.516; V_0, 2 V (○), 4 V (●), 10 V (□); i_d, 0.115 mA cm^{-1} (○), 0.229 mA cm^{-1} (●), 0.573 mA cm^{-1} (□).

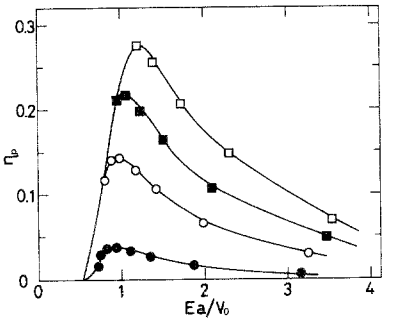

Fig. 15. Power efficiency, η_P, plotted against Ea/V_0 for different values of $i_d a/V_0\kappa$ for the B-type arrangement. r/a, 0.5; $i_d a/V_0\kappa$, 0.0516 (●), 0.258 (○), 0.516 (■), 1.031 (□).

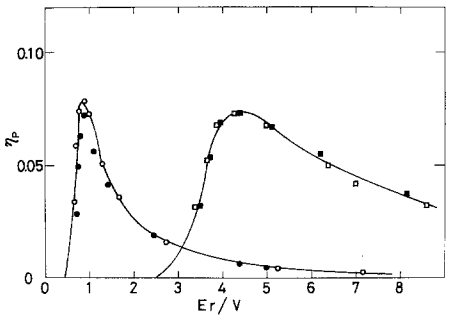

Fig. 16. Power efficiency, η_P, plotted against Er for A- and B-type arrangements. Type of arrangement: A (●, ■); B (○, □). V_0: 2 V (●, ○), 10 V (■, □). i_d: 0.1 mA cm^{-1} (●, ○), 0.5 mA cm^{-1} (■, □).

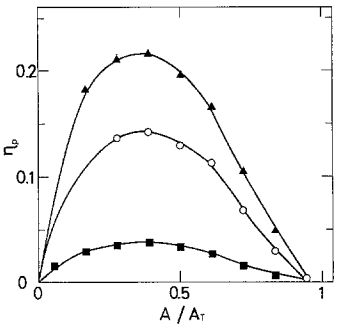

Fig. 17. Relationship between η_P and A/A_T for different values of $i_d a/V_0\kappa$ for the B-type arrangement. r/a, 0.5; $i_d a/V_0\kappa$, 0.0516 (■), 0.258 (○), 0.516 (▲).

5. Conclusion

A new method of simulating a packed bipolar cell has been described, and cell characteristics such as A/A_T and η_P have been obtained for different values of r/a, $i_d a/V_0\kappa$ and Ea/V_0. The combination of the conducting paper and the electric circuit can be modified to simulate more general cases where the current–potential relationship is not symmetric for anodic and cathodic reactions, that is, $i_a \neq i_c$. It may also be possible to make electric circuits which simulate non-diffusion-controlled behaviours, e.g. a Tafel-type current–potential relationship.

The method described in this paper may be applicable to the simulation of the potential distribution and current distribution in other types of electrolysers. An advantage of this method is that it can simulate cells of complex geometry for which computer simulation is too complicated.

References

[1] M. Fleischmann, J. W. Oldfield and C. L. K. Tennakoon, 'The Electrochemical Bipolar Particulate Cell', Symposium on the Electrochemical Engineering, Newcastle upon Tyne (1971); Proceedings, Vol. 1, The Institution of Chemical Engineers, London (1973) p. 53; *Chem. Abstr.* **80** (1974) 55276b.
[2] A. B. Smith and M. J. Hayes, Ger. Offen., 1949129, 9 April 1970; US Application, 1 October 1968; *Chem. Abstr.* **72** (1970) 124900z.
[3] S. Yoshizawa, Y. Miyazaki and A. Katagiri, *Nippon Kagaku Kaishi* (1977) 19; *Chem. Abstr.* **86** (1977) 126710a.
[4] S. Yoshimura, A. Katagiri and S. Yoshizawa, *Nippon Kagaku Kaishi* (1978) 1144; *Chem. Abstr.* **89** (1978) 203641v.
[5] S. Motozawa, Japan. Patent 78 35867, 29 September 1978; *Chem. Abstr.* **86** (1977) 130035b.
[6] T. Sawa, M. Kubota, S. Takahashi and Y. Masaki, *Desalination* **32** (1980) 373.
[7] F. Goodridge, C. J. H. King and A. R. Wright, *Electrochim. Acta* **22** (1977) 347.
[8] Y. Miyazaki, A. Katagiri and S. Yoshizawa, unpublished work.
[9] J. Newman, 'Electrochemical Systems', Prentice Hall, Englewood Cliffs, NJ (1973) pp. 340–52.
[10] S. Yoshizawa (ed), 'Denki Kagaku', Vol. 3, Kyoritsu-Shuppan, Tokyo (1974), pp. 189–205.
[11] M. Takahashi, and N. Masuko, 'Kogyodenkai no Kagaku', Agune Tokyo (1979) pp. 135–53; pp. 269–74.
[12] F. Hine, 'Electrode Processes and Electrochemical Engineering', Plenum Press, New York (1985) pp. 313–38.